Magazine of Civil Engineering. 2025. 18(3). Article No. 13502

Magazine of Civil Engineering

ISSN 2712-8172

journal homepage: http://engstroy.spbstu.ru/

Research article

UDC 624.04

DOI: 10.34910/MCE.135.2

Rectangular flat finite element for modeling the process of crack formation

Yu.Ya. Tyukalov ✉

Vyatka State University, Kirov, Russian Federation

✉ *yutvgu@mail.ru*

Keywords: finite element method, crack width, tensile strength, stiffness matrix, possible displacements, crack tip

Abstract. A rectangular flat finite element is proposed that allows modeling the process of crack formation without changing the initial elements' grid. The proposed finite element can be used to calculate structures made of reinforced concrete, masonry, fiber concrete, and other materials with low tensile strength. To calculate structures with existing cracks, their position can be specified as initial data. The finite element was formed based on the stress fields approximations and the principle of possible displacements to obtain the equilibrium equations of nodes. To calculate the stiffness matrix of the finite element, the principle of minimum additional energy was used, to which algebraic equilibrium equations were added using the Lagrange multiplier method. After a crack formation in the centre of finite element, additional degrees of freedom were introduced into its nodes, determining the possible mutual displacement of the element's parts separated by the crack. The calculations were performed for a rectangular elastic bending beam with a low tensile strength. The reinforcement was located in the tensile zone of the beam. For comparison, the beam was also calculated using standard finite elements. The comparison of the results, including the crack width, for the two solutions showed that they coincided with high accuracy. The maximum displacements differ by 1.5 %, the maximum stresses in compressed concrete and reinforcement differ by less than 1 %. The crack width for the two solutions differs by no more than 5–7 %.

Citation: Tyukalov, Yu.Ya. Rectangular flat finite element for modeling the process of crack formation. Magazine of Civil Engineering. 2025. 18(3). Article no. 13502. DOI: 10.34910/MCE.135.2

1. Introduction

In the construction of industrial and civil buildings, materials such as reinforced concrete and masonry are widely used. Such materials have low tensile strength, so cracks occur in them. The formation and growth of cracks causes a redistribution of forces and stresses in the structural elements. A number of scientific articles are devoted to the problem of calculating structures with cracks [1–3]. In [2, 4, 5], Extended Finite Element Method (XFEM) and substructure methods were used for crack modeling. In [2], the structures are divided into several substructures, and XFEM is employed to model the presence of cracks within each substructure. To evaluate the proposed method, four examples have been considered. In [6], a finite element formulation is developed that modeled a local crack as imposed strain to simulate fracture in quasi-brittle materials. For simplicity, only tensile crack has been considered. The structure is modeled as an averaged continuum, using constant strain triangles. Cracks can develop along the element edges by controlling the forces normal to the potential crack direction at the nodes. In [7], a novel local mesh refinement numerical manifold method with variable-midside-node elements for fracture analysis in solids is presented. In the framework of conventional numerical manifold method, a local mesh refinement algorithm was proposed to achieve automatic multilevel refinement to the original coarse mesh in a focused region. In [8], a constitutive model coupling the rotating smeared crack model and the plasticity model in incremental sequentially linear analysis is proposed.

In [9], the sequentially linear approach based on the exponential softening is proposed to solve the divergence problem of computational process due to negative stiffness encountered in fracture analysis of concrete or masonry structure, and nonlinear response is obtained through several linear analyses. In [10–13], the formation of cracks in various beam systems is investigated. The article [10] presents a novel strain-based beam finite element family for the analysis of softening and localization of longitudinal deformations in planar frames made of brittle materials. In the analysis, the softening region was limited only to a discrete crack, which was treated as an “exclude” element point, i.e., the deformation quantities in the crack were considered separately from the deformations in the immediate vicinity of the crack. Localized deformations are connected to the element only through kinematic quantities, which used to describe the crack opening. The problem of analyzing the stress-strain state of shells, plates and nodal connections taking into account cracks is investigated in [14–17]. In [17], an innovative fiber beam-column model updating method based on static deflection and crack width is proposed. The fiber beam-column finite element program COMPONA-MARC, developed in this laboratory, is modified to efficiently simulate the nonlinear cracking behavior of reinforced concrete flexural members.

A large number of scientific papers are devoted to the study of crack propagation based on fracture mechanics [18–20]. In [18], a numerical model for wing crack initiation and propagation due to shear slip is presented. The governing mathematical model is based on linear elastic fracture mechanics and contact mechanics, along with failure and propagation criteria for multiple mixed-mode fracture propagation. The numerical solution approach is based on a combination of the finite element method combined with quarter point elements to handle the singularity at the fracture tips. In [21], a method to achieve smooth nodal stresses in the XFEM application is presented. The salient feature of the method is to introduce an “average” gradient into the construction of the approximation, resulting in improved solution accuracy, both in the vicinity of the crack tip and in the far field. Due to the higher-order polynomial basis provided by the interpolants, the new approximation enhances the smoothness of the solution without requiring an increased number of degrees of freedom. An alternative formulation of the finite element method, which is based on stress approximations, is presented in [22–25]. The solution is based on the additional energy functional, to which, using the Lagrange multiplier method, the algebraic equilibrium equations of the finite element mesh nodes are added. The equilibrium equations are constructed with the principle of possible displacements.

In [26], a new finite element formulation for the analysis of reinforced concrete slabs is proposed, accounting for concrete cracking and reinforcement yielding. The proposed formulation, developed within the framework of Lumped Damage Mechanics, considers that all inelastic effects **are** localized in lines and relates all numerical parameters to the mechanical properties of the slab. The problem of formation and propagation of cracks in bending plates is studied in [27–29]. In [27], the crack is modelled as a rotational spring with additional rotational freedoms being added to the finite element nodes. The method is validated against published results for through-the-depth cracks. Cracks with varying direction, location, depth, and length are used to study the effects of changing the crack parameters. A novel refined numerical method for simulating cross-scale crack propagation in 3D massive concrete structure is proposed in [30]. The applicability of the proposed method is verified by a three-point bending test of the beam with regular and irregular cracks. Finally, the simulation analysis of the roller-compacted concrete dam with cross-scale irregular cracks is performed based on the monitoring cracks. The modifications of the traditional finite element method that allow modeling the formation and propagation of cracks are presented in [31, 32]. In [33], an innovation is proposed to use precise shell-solid finite element models to study the redistribution factor of composite frame structures under horizontal loads considering concrete cracking. Using shell-solid finite element models, the cracking behavior due to the slab spatial composite effect can be considered. In [34], the strain compliance crack model is proposed to capture, as reported by tests, the specifics of various cases of crack spacing and width analysis involving primary and secondary cracks in reinforced concrete beams. The model dwells on calculating crack spacing based on the reinforcement strain profile. The works [35–37] also present methods for solving stability and statics problems based on stress approximation, as well as mixed approximations.

The problem of developing methods for calculating building structures taking into account the process of crack formation remains relevant. The largest number of scientific articles are devoted to studies of the crack propagation under constant load based on fracture mechanics. The purpose of this work is to develop a flat finite element that will allow modeling the process of crack formation under loading without changing the finite element mesh.

2. Methods

Stiffness matrix of an equilibrium rectangular finite element without a crack.

To construct the stiffness matrix, we use the following stresses approximations over a finite element domain:

$$\sigma_x = a_1 + a_4 y, \ \ \sigma_y = a_2 + a_5 x, \ \ \tau_{xy} = a_3. \tag{1}$$

Similar approximations were used in [35] to construct a flat finite element of arbitrary shape. Thus, the shear stresses are constant in the finite element region, and the normal stresses along the X and Y axes vary linearly. The stress approximations (1) satisfy the homogeneous differential equations of equilibrium of the plane problem of elasticity theory.

Let us write expressions (1) in matrix form:

$$\sigma = \mathbf{H}\mathbf{a}, \ \ \sigma = \begin{Bmatrix} \sigma_x \\ \sigma_y \\ \tau_{xy} \end{Bmatrix}, \ \ \mathbf{H} = \begin{bmatrix} 1 & 0 & 0 & y & 0 \\ 0 & 1 & 0 & 0 & x \\ 0 & 0 & 1 & 0 & 0 \end{bmatrix}, \ \ \mathbf{a} = \begin{Bmatrix} a_1 \\ a_2 \\ a_3 \\ a_4 \\ a_5 \end{Bmatrix}. \tag{2}$$

Consider the stiffness matrix construction of a rectangular finite element (Fig. 1), which will be used later to model the process of crack formation in the structure tension zones.

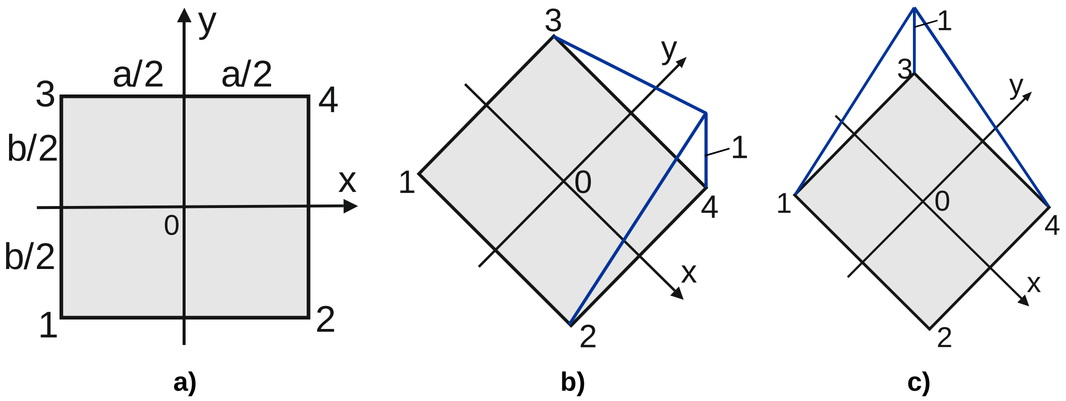

Figure 1. Rectangular finite element: a) coordinate system; b) possible displacement of node 4; c) possible displacement of node 3.

The nodal unknowns vector includes the displacements of a node along the X and Y axes, respectively:

$$\mathbf{u}_i^{\mathrm{T}} = \left(u_{x,i} \ \ u_{y,i} \right). \tag{3}$$

The stiffness matrix is obtained using the principles of minimum additional energy and possible displacements. The principle of possible displacements is written as follows:

$$\delta \mathrm{U}_i + \delta \mathrm{V}_i = 0, \tag{4}$$

where $\delta \mathrm{U}_i$ is the deformations energy with possible displacement of the node; $\delta \mathrm{V}_i$ is the potential of nodal reactions, equal to the work of the reaction taken with a minus sign.

By considering the possible displacements of nodes, we can obtain algebraic equilibrium equations for them. To approximate the possible displacements vector over the finite element domain, we use the following functions:

$$\delta u_x = \delta u_y = N_i\left(x, y\right) = \frac{1}{4}\left(1 + \frac{4xx_i}{a^2}\right)\left(1 + \frac{4yy_i}{b^2}\right), \ \ i = 1, 2, 3, 4. \tag{5}$$

where x_i, y_i are the nodal point coordinates in the local coordinate system (Fig. 1). Using (5), we obtain expressions for the deformations corresponding to the possible displacement of the node along the X axis:

$$\delta\varepsilon_x = \frac{\partial N_i\left(x, y\right)}{\partial x} = \frac{x_i}{a^2}\left(1 + \frac{4yy_i}{b^2}\right), \ \ \delta\tau_{xy} = \frac{\partial N_i\left(x, y\right)}{\partial y} = \frac{y_i}{b^2}\left(1 + \frac{4xx_i}{a^2}\right). \tag{6}$$

And with the possible displacement of the node along the Y axis, we obtain, respectively:

$$\delta\varepsilon_y = \frac{\partial N_i(x,y)}{\partial y} = \frac{y_i}{b^2}\left(1+\frac{4xx_i}{a^2}\right),\ \ \delta\tau_{xy} = \frac{\partial N_i(x,y)}{\partial x} = \frac{x_i}{a^2}\left(1+\frac{4yy_i}{b^2}\right). \tag{7}$$

The deformation energy for possible displacement of node i along the X axis:

$$\delta\mathrm{U}_{i,x} = t\int_{-b/2}^{b/2}\int_{-a/2}^{a/2}\left(\sigma_x\delta\varepsilon_x + \tau_{xy}\delta\gamma_{xy}\right)\mathrm{d}x\mathrm{d}y = a_1\frac{tbx_i}{a} + a_4\frac{tbx_iy_i}{3a} + a_3\frac{tay_i}{b}, \tag{8}$$

where t is the finite element thickness.

Similarly, we obtain the deformation energy expression for the possible displacement along the Y axis:

$$\delta\mathrm{U}_{i,y} = t\int_{-b/2}^{b/2}\int_{-a/2}^{a/2}\left(\sigma_y\delta\varepsilon_y + \tau_{xy}\delta\gamma_{xy}\right)\mathrm{d}x\mathrm{d}y = a_2\frac{tay_i}{b} + a_5\frac{tax_iy_i}{3b} + a_3\frac{tbx_i}{a}. \tag{9}$$

We write the equilibrium equations (3) for node i in a matrix form:

$$\mathbf{L}_i\mathbf{a} - \mathbf{R}_i = 0; \tag{10}$$

$$\mathbf{L}_i = \begin{bmatrix} \dfrac{tbx_i}{a} & 0 & \dfrac{tay_i}{b} & \dfrac{tbx_iy_i}{3a} & 0 \\ 0 & \dfrac{tay_i}{b} & \dfrac{tbx_i}{a} & 0 & \dfrac{tax_iy_i}{3b} \end{bmatrix},\ \ \mathbf{R}_i = \begin{Bmatrix} R_{i,x} \\ R_{i,y} \end{Bmatrix}. \tag{11}$$

The system of equilibrium equations for all nodes of the element has the following form:

$$\mathbf{La} - \mathbf{R} = 0,\ \ \mathbf{L} = \begin{bmatrix} \mathbf{L}_1 \\ \mathbf{L}_2 \\ \mathbf{L}_3 \\ \mathbf{L}_4 \end{bmatrix},\ \ \mathbf{R} = \begin{Bmatrix} \mathbf{R}_1 \\ \mathbf{R}_2 \\ \mathbf{R}_3 \\ \mathbf{R}_4 \end{Bmatrix}. \tag{12}$$

Let us introduce the notation for the material stiffness matrix:

$$\mathbf{E}^{-1} = \frac{t}{E}\begin{bmatrix} 1 & -\mu & 0 \\ -\mu & 1 & 0 \\ 0 & 0 & 2(1+\mu) \end{bmatrix}, \tag{13}$$

where $\mathrm{E},\ \mu$ are the elasticity modulus and Poisson's ratio of the material. We represent the deformations additional energy of the finite element in the following form:

$$\mathrm{E} = \frac{1}{2}\mathbf{a}^{\mathrm{T}}\mathbf{Da} \to \min,\ \ \mathbf{D} = \int_{-b/2}^{b/2}\int_{-a/2}^{a/2}\mathbf{H}^{\mathrm{T}}\mathbf{E}^{-1}\mathbf{H}\mathrm{d}x\mathrm{d}y; \tag{14}$$

$$\mathbf{D} = \frac{abt}{\mathrm{E}}\begin{bmatrix} 1 & -\mu & 0 & 0 & 0 \\ -\mu & 1 & 0 & 0 & 0 \\ 0 & 0 & 2(1+\mu) & 0 & 0 \\ 0 & 0 & 0 & \dfrac{b^2}{12} & 0 \\ 0 & 0 & 0 & 0 & \dfrac{a^2}{12} \end{bmatrix}. \tag{15}$$

Using the Lagrange multiplier method, we add the equilibrium equations (12) to the functional (14):

$$\mathrm{E}=\frac{1}{2}\mathbf{a}^{\mathrm{T}}\mathbf{D}\mathbf{a}+\mathbf{u}^{\mathrm{T}}\left(\mathbf{L}\mathbf{a}-\mathbf{R}\right)\rightarrow\min. \tag{16}$$

By equating the derivatives of expression (16) with respect to vectors $\mathbf{a}$ and $\mathbf{u}$, we obtain the following equations:

$$\mathbf{D}\mathbf{a}+\mathbf{L}^{\mathrm{T}}\mathbf{u}=0,\ \ \mathbf{L}\mathbf{a}-\mathbf{R}=0. \tag{17}$$

Expressing the vector from the first equation $\mathbf{a}$ and substituting it into the second equation, we obtain:

$$\mathbf{a}=-\mathbf{D}^{-1}\mathbf{L}^{\mathrm{T}}\mathbf{u}; \tag{18}$$

$$\mathbf{K}\mathbf{u}=\mathbf{R}; \tag{19}$$

$$\mathbf{K}=\mathbf{L}\mathbf{D}^{-1}\mathbf{L}^{\mathrm{T}}. \tag{20}$$

Thus, the expression for the stiffness matrix of the finite element $\mathbf{K}$ is obtained. Note that the matrix consists of 8 rows and columns.

Stiffness matrix of an equilibrium rectangular finite element with a crack.

We obtain an expression for the finite element stiffness matrix after a crack has formed in it. We agree that a crack is formed if the maximum principal stress at the finite element center reaches the material tensile strength $\mathrm{R_t}$. At the center of the finite element, the coordinates (x, y) are zero, so the stresses are determined by only three parameters:

$$\sigma_x=a_1,\ \ \sigma_y=a_2,\ \ \tau_{xy}=a_3. \tag{21}$$

The maximum principal stress at the finite element center and the crack inclination angle will be determined by the following well-known expressions:

$$\sigma_1=\frac{\sigma_x+\sigma_y}{2}+\sqrt{\frac{\left(\sigma_x-\sigma_y\right)^2}{4}+\tau_{xy}^2}\geq\mathrm{R_t}; \tag{22}$$

$$\alpha_{cr}=\frac{1}{2}\,\mathrm{acrtg}\frac{2\tau_{xy}}{\left(\sigma_x-\sigma_y\right)}. \tag{23}$$

Depending on the inclination angle, there are two possible options for the crack location in the element. In the first option, the nodes 1 and 3 are located on one crack side, and the nodes 2 and 4 are located on the other. In the second variant, the nodes 1 and 2 are located on one side, and the nodes 3 and 4 are located on the other side (Fig. 2).

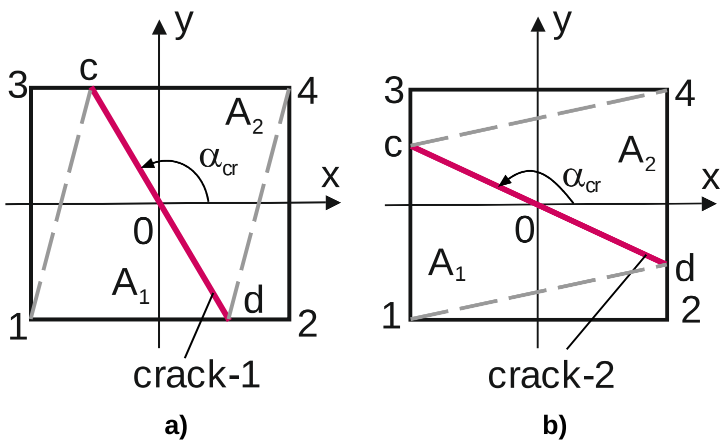

Figure 2. Variants of crack cd location.

Consider the first variant of the crack location. After the crack has formed, we introduce additional degrees of freedom into the nodes of the finite element. These degrees of freedom are associated with the possibility of shifting two parts of the element A_1 and A_2, separated by a crack, relative to each other. Thus, after the crack formation, the number of degrees of freedom in the nodes of the finite element increases. Let us denote the vector of additional degrees of freedom in node i:

$$\mathbf{u}_i^{cr} = \begin{Bmatrix} u_{i,x}^{cr} \\ u_{i,y}^{cr} \end{Bmatrix}. \tag{24}$$

To approximate the possible displacements of the main and additional degrees of freedom of the nodes, we also use functions (5). Fig. 3 shows the displacement functions from the main and additional possible displacements of nodes 3 and 4.

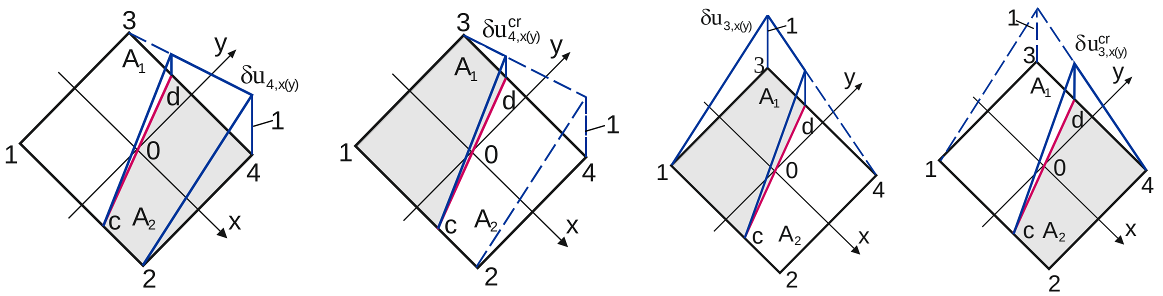

Figure 3. Main and additional possible displacements of nodes after the crack cd formation:

a) $\delta u_{4,x(y)}$; **b)** $\delta u_{3,x(y)}$; **c)** $\delta u_{4,x(y)}^{cr}$; **d)** $\delta u_{3,x(y)}^{cr}$.

After the crack has formed, the main possible displacements of the node cause displacements only in the region of the finite element adjacent to this node. This region is limited by the crack line. The additional possible displacements cause displacements and deformations only in the opposite region of the finite element, located behind the crack line (Fig. 3b). In both cases, the same functions (5) are used to approximate the possible displacements. The possible displacements of nodes 1 and 2 are accepted similarly.

Due to the discontinuity of displacements and deformations, the number of parameters required to approximate the stresses increases. The stresses approximate parameters are different in the two regions of the finite element (25):

$$\mathbf{a}^{\mathrm{T}} = \left(a_1^1 \;\; a_2^1 \;\; a_3^1 \;\; a_4^1 \;\; a_5^1 \;\; a_1^2 \;\; a_2^2 \;\; a_3^2 \;\; a_4^2 \;\; a_5^2 \right). \tag{25}$$

The first five parameters are used to approximate the stresses in the region A_1, the remaining five are used to approximate the stresses in the region A_2. Expressions (1) are used to approximate the stresses in each region of the finite element.

When calculating the deformation energy, integration is performed only over a part of the finite element. For example, for the main possible displacement of node i along the X axis, the deformation energy is calculated using the following formula:

$$\delta \mathrm{U}_{i,x} = t \int\limits_{\mathrm{A}_i} \left(\sigma_x \delta\varepsilon_x + \tau_{xy} \delta\gamma_{xy} \right) d\mathrm{A}, \;\; \mathrm{A}_i = \begin{cases} \mathrm{A}_1, \; i = 1,3 \\ \mathrm{A}_2, \; i = 2,4 \end{cases}. \tag{26}$$

For additional possible displacement along the X axis, integration is performed over the opposite region of the finite element relative to the crack:

$$\delta \mathrm{U}_{i,x}^{cr} = t \int\limits_{\mathrm{A}_i} \left(\sigma_x \delta\varepsilon_x + \tau_{xy} \delta\gamma_{xy} \right) d\mathrm{A}, \;\; \mathrm{A}_i = \begin{cases} \mathrm{A}_1, \; i = 2,4 \\ \mathrm{A}_2, \; i = 1,3 \end{cases}. \tag{27}$$

For integration, the quadrangular region is divided into two triangles, indicated in Fig. 2 by a dotted line. For each triangular region, the integrals were calculated analytically using triangular coordinates. Let us introduce for the domain A_1 the designations of the necessary integrals, calculated analytically:

$$\mathrm{I}_x^1 = \int\limits_{13c} x\mathrm{dA} + \int\limits_{1cd} x\mathrm{dA},\ \mathrm{I}_y^1 = \int\limits_{13c} y\mathrm{dA} + \int\limits_{1cd} y\mathrm{dA},\ \mathrm{I}_{xy}^1 = \int\limits_{13c} xy\mathrm{dA} + \int\limits_{1cd} xy\mathrm{dA},$$
$$\mathrm{I}_{xx}^1 = \int\limits_{13c} x^2\mathrm{dA} + \int\limits_{1cd} x^2\mathrm{dA},\ \mathrm{I}_{yy}^1 = \int\limits_{13c} y^2\mathrm{dA} + \int\limits_{1cd} y^2\mathrm{dA}. \tag{28}$$

The similar designations are adopted for the region A_2: $\mathrm{I}_x^2,\ \mathrm{I}_y^2,\ \mathrm{I}_{xx}^2,\ \mathrm{I}_{yy}^2,\ \mathrm{I}_{xy}^2$. Using (26), we obtain the matrix $\mathbf{L}_i$ elements for the main possible displacement of node i:

$$\mathbf{L}_i = \\ = \begin{bmatrix} \frac{x_i}{a^2}\left(\mathrm{A}_k + \frac{4y_i}{b^2}\mathrm{I}_y^k\right) & 0 & \frac{y_i}{b^2}\left(\mathrm{A}_k + \frac{4x_i}{a^2}\mathrm{I}_x^k\right) & \frac{x_i}{a^2}\left(\mathrm{I}_y^k + \frac{4y_i}{b^2}\mathrm{I}_{yy}^k\right) & 0 \\ 0 & \frac{y_i}{b^2}\left(\mathrm{A}_k + \frac{4x_i}{a^2}\mathrm{I}_x^k\right) & \frac{x_i}{a^2}\left(\mathrm{A}_k + \frac{4y_i}{b^2}\mathrm{I}_y^k\right) & 0 & \frac{y_i}{b^2}\left(\mathrm{I}_x^k + \frac{4x_i}{a^2}\mathrm{I}_{xx}^k\right) \end{bmatrix}, \\ k = \begin{cases} 1,\ i = 1,3 \\ 2,\ i = 2,4 \end{cases}. \tag{29}$$

The matrix $\mathbf{L}_i^{cr}$ elements for additional possible displacement are calculated by changing the index k values to the opposite values:

$$\mathbf{L}_i^{cr} = \\ = \begin{bmatrix} \frac{x_i}{a^2}\left(\mathrm{A}_k + \frac{4y_i}{b^2}\mathrm{I}_y^k\right) & 0 & \frac{y_i}{b^2}\left(\mathrm{A}_k + \frac{4x_i}{a^2}\mathrm{I}_x^k\right) & \frac{x_i}{a^2}\left(\mathrm{I}_y^k + \frac{4y_i}{b^2}\mathrm{I}_{yy}^k\right) & 0 \\ 0 & \frac{y_i}{b^2}\left(\mathrm{A}_k + \frac{4x_i}{a^2}\mathrm{I}_x^k\right) & \frac{x_i}{a^2}\left(\mathrm{A}_k + \frac{4y_i}{b^2}\mathrm{I}_y^k\right) & 0 & \frac{y_i}{b^2}\left(\mathrm{I}_x^k + \frac{4x_i}{a^2}\mathrm{I}_{xx}^k\right) \end{bmatrix}, \\ k = \begin{cases} 1,\ i = 2,4 \\ 2,\ i = 1,3 \end{cases}. \tag{30}$$

The matrix of equilibrium equations, which are similar (12), for a finite element is composed of the matrices (29) and (30):

$$\mathbf{L} = \begin{bmatrix} \mathbf{L}_1 & \mathbf{O} \\ \mathbf{O} & \mathbf{L}_2 \\ \mathbf{L}_3 & \mathbf{O} \\ \mathbf{O} & \mathbf{L}_4 \\ \mathbf{O} & \mathbf{L}_1^{cr} \\ \mathbf{L}_2^{cr} & \mathbf{O} \\ \mathbf{O} & \mathbf{L}_3^{cr} \\ \mathbf{L}_4^{cr} & \mathbf{O} \end{bmatrix}. \tag{31}$$

The matrix consists of 10 columns, corresponding to different stress approximation parameters, and 16 rows, corresponding to the node's possible displacements.

For the second crack variant (Fig. 2), in expressions (29) and (30), it is necessary for the parameter k to replace the pair of indices 1.3 with the pair 1.2 and the indices 2.4 with the pair 3.4. In addition, in (31), the position of the matrices $\mathbf{L}_i,\ \mathbf{L}_i^{cr}$ must be changed to the following:

$$\mathbf{L}=\begin{bmatrix}\mathbf{L}_1 & \mathbf{O}\\ \mathbf{L}_2 & \mathbf{O}\\ \mathbf{O} & \mathbf{L}_3\\ \mathbf{O} & \mathbf{L}_4\\ \mathbf{O} & \mathbf{L}_1^{cr}\\ \mathbf{O} & \mathbf{L}_2^{cr}\\ \mathbf{L}_3^{cr} & \mathbf{O}\\ \mathbf{L}_4^{cr} & \mathbf{O}\end{bmatrix}. \quad (32)$$

The matrix $\mathbf{D}$, similar to (13), has the following form:

$$\mathbf{D}=\begin{bmatrix}\mathbf{D}_1 & \mathbf{O}\\ \mathbf{O} & \mathbf{D}_2\end{bmatrix}. \quad (33)$$

$$\mathbf{D}_i=\frac{t}{\mathrm{E}}\begin{bmatrix}\mathrm{A}_i & -\mu\mathrm{A}_i & 0 & \mathrm{I}_y^i & -\mu\mathrm{I}_x^i\\ & \mathrm{A}_i & 0 & -\mu\mathrm{I}_y^i & \mathrm{I}_x^i\\ & & 2(1+\mu) & 0 & 0\\ & \text{symmetric} & & \mathrm{I}_{yy}^i & -\mu\mathrm{I}_{xy}^i\\ & & & & \mathrm{I}_{xx}^i\end{bmatrix}. \quad (34)$$

The finite element stiffness matrix is also calculated by formula (20) and contains 16 rows and columns. The A global stiffness matrix for all structure is formed from the matrix stiffness of the finite elements.

Depending on the presence of cracks in the finite elements, there may be 2, 4 or 6 unknowns in a node. If there are no cracks in all elements surrounding the node, then there are only two unknowns in the node. If there are cracks in elements only to the right (bottom) or left (top) of the node, then there are four unknowns in the node. If there are cracks in the elements located to the right and left (bottom and top) of the node, then there are six unknowns in the node (Fig. 4).

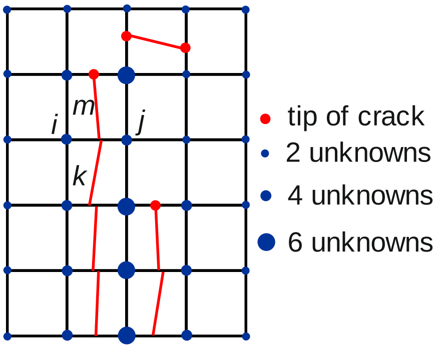

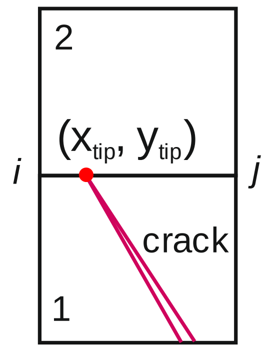

Figure 4. Cracks: a) the unknowns' number in a node, depending on the cracks location; b) the tip of a crack.

The determination of crack opening width.

For a finite element, the crack opening width is determined at points c and d in the direction to the crack normal (Fig. 2). The width of the crack opening in the direction of the local axes X and Y is determined by the difference in the displacements of its sides, according to the following formulas:

$$w_{c,x}^{cr}=u_{4,x}N_4(x_c,y_c)+u_{3,x}^{cr}N_3(x_c,y_c)-u_{3,x}N_3(x_c,y_c)-u_{4,x}^{cr}N_4(x_c,y_c); \quad (35)$$

$$w_{c,y}^{cr} = u_{4,y} N_4 \left(x_c, y_c \right) + u_{3,y}^{cr} N_3 \left(x_c, y_c \right) - u_{3,y} N_3 \left(x_c, y_c \right) - u_{4,y}^{cr} N_4 \left(x_c, y_c \right). \quad (36)$$

Then, the crack width in the direction of the normal to it is equal to:

$$w_{c,n}^{cr} = w_{c,x}^{cr} \cos\left(\alpha_{cr} - \pi/2 \right) + w_{c,y}^{cr} \sin\left(\alpha_{cr} - \pi/2 \right). \quad (37)$$

For point d, the crack width is determined similarly:

$$w_{d,x}^{cr} = u_{2,x} N_2 \left(x_d, y_d \right) + u_{1,x}^{cr} N_1 \left(x_d, y_d \right) - u_{1,x} N_1 \left(x_d, y_d \right) - u_{1,x}^{cr} N_2 \left(x_d, y_d \right); \quad (38)$$

$$w_{d,y}^{cr} = u_{2,y} N_2 \left(x_d, y_d \right) + u_{1,y}^{cr} N_1 \left(x_d, y_d \right) - u_{1,y} N_1 \left(x_d, y_d \right) - u_{1,y}^{cr} N_2 \left(x_d, y_d \right); \quad (39)$$

$$w_{d,n}^{cr} = w_{d,x}^{cr} \cos\left(\alpha_{cr} - \pi/2 \right) + w_{d,y}^{cr} \sin\left(\alpha_{cr} - \pi/2 \right). \quad (40)$$

The closing of crack edges at its tip.

The crack tip is located at the boundary of two finite elements, one of which has no crack (Fig. 4). At the top of the crack, its banks come together (Fig. 4b). The vertical and horizontal displacements of the crack tip in element 1 must be equal to the corresponding displacements of this point in finite element 2, in which there is no crack. In the element 2, the displacements of the crack tip are determined only by the main displacements of nodes i and j:

$$u_{x,tip} = u_{i,x} N_i \left(x_{tip}, y_{tip} \right) + u_{j,x} N_j \left(x_{tip}, y_{tip} \right); \quad (41)$$

$$u_{y,tip} = u_{i,y} N_i \left(x_{tip}, y_{tip} \right) + u_{j,y} N_j \left(x_{tip}, y_{tip} \right). \quad (42)$$

In finite element 1, the displacements of the crack sides are determined by the main and additional displacements of one of the nodes i or j. The displacements of the crack tip on the left side are expressed through the displacements of node i:

$$u_{x,tip}^{left} = u_{i,x} N_i \left(x_{tip}, y_{tip} \right) + u_{j,x}^{cr} N_j \left(x_{tip}, y_{tip} \right); \quad (43)$$

$$u_{y,tip}^{left} = u_{i,y} N_i \left(x_{tip}, y_{tip} \right) + u_{j,y}^{cr} N_j \left(x_{tip}, y_{tip} \right). \quad (44)$$

Equating expressions (41) and (42) to expressions (43) and (44), respectively, we obtain:

$$u_{j,x}^{cr} = u_{j,x}, \;\; u_{j,y}^{cr} = u_{j,y}. \quad (45)$$

Considering the displacements of the crack tip on the right side, we obtain:

$$u_{i,x}^{cr} = u_{i,x}, \;\; u_{i,y}^{cr} = u_{i,y}. \quad (46)$$

Equalities (45) and (46) mean that the corresponding additional and main unknowns at the nodes belonging to the side on which the crack tip is located must be equal to each other. Simply assigning the same numbers to the corresponding main and additional unknowns ensures equalities (45) and (46).

The iterative algorithm for the problem solving.

In this article, we consider an algorithm for solving the problem for the case of a linear $\sigma\left(\varepsilon\right)$ diagram shown in Fig. 5.

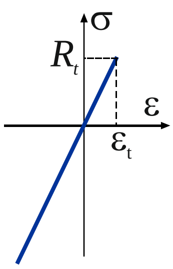

Figure 5. Material deformation diagram.

A material corresponding to such a diagram is elastic, but if the tensile stresses reach the tensile strength, brittle failure occurs and a crack appears. The nonlinear behavior of a structure made of such material is determined by the successive occurrence of cracks in the tension zones. The main stages of the iterative solution are shown in Fig. 6.

1. Compute the number of unknowns n_d and the tape width of the equation system l_d.

2. Accept $\mathbf{u} = \mathbf{0}$.

3. Compute the load vector $\mathbf{R}$.

4. Compute the elements of stiffness matrix $\mathbf{K}(\mathbf{u})$.

5. Solve the linear equation system $\mathbf{Ku} = \mathbf{R}$.

6. Compute the vector of first principal stresses of the finite element centers $\mathbf{S}_1$.

7. Find the element of vector $\mathbf{S}_1$ with the maximum value s_i.

8. If $s_i \geq \mathrm{R}_t$, then:

8.1. Add the additional unknowns u^{cr} into the nodes of the finite element *i*.

8.2. Recompute the number of unknowns n_d and tape width l_d of the equation system.

8.3. Recompute the load vector $\mathbf{R}$.

8.4. Go to line 4.

9. Compute the stresses of finite elements $\boldsymbol{\sigma}$ and width of cracks $\mathbf{w}_{\mathrm{cr}}$.

10. Exit.

Figure 6. Iterative solution algorithm.

The iterative algorithm allows determining the sequence of crack formation. When a new crack is formed, additional unknowns are added to the nodes of the finite element if the corresponding unknowns were not added to these nodes in previous iterations. For example, if a crack has formed in element m (Fig. 4a), and in element k a crack has formed in previous iterations, then there is no need to introduce additional unknowns into nodes i and j. During the iterations, the numbers of finite elements, in which cracks have formed, are noted. If new cracks do not form, then the solution is obtained and the iterations are finished. The number of necessary iterations is determined by the number of cracks that can occur under the given loads.

3. Results and Discussion

As a test, calculation of a bending, hinged beam was performed for the action of a uniformly distributed load. The beam length is 6 m. Half of the beam was calculated. To increase the beam rigidity, reinforcement is added to the stretched zone. The reinforcement is located at a distance of 30 mm from the lower edge. The reinforcement is modeled by rod finite elements working in tension and compression. The characteristics of the beam are given in Table 1.

Table 1. Beam parameters.

Beam						Reinforcement		
0.5L, m	h, m	t, m	E, kPa	R_t, kPa	μ	h_0, m	E_a, kPa	A_a, m^2
3	0.6	0.4	30000000	1140	0.25	0.57	200000000	0.003

The beam was divided by height into 20 and by length into 40 finite elements (Fig. 7). Along line AB, vertical displacements at the nodes were excluded, and along line CD, horizontal displacements were excluded. A uniformly distributed load was applied of the beam upper edge in the form of concentrated forces to the nodes.

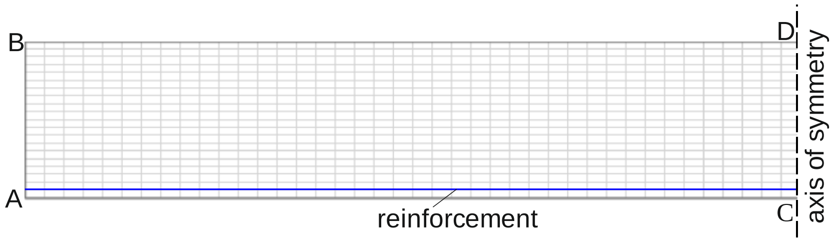

Figure 7. Finite elements mesh and reinforcement of proposed (Cr-FE).

Fig. 8 shows the position and size of crack opening, as well as the stresses in the reinforcement at different values of uniformly distributed load q. From Fig. 8, one can trace the sequence of crack formation.

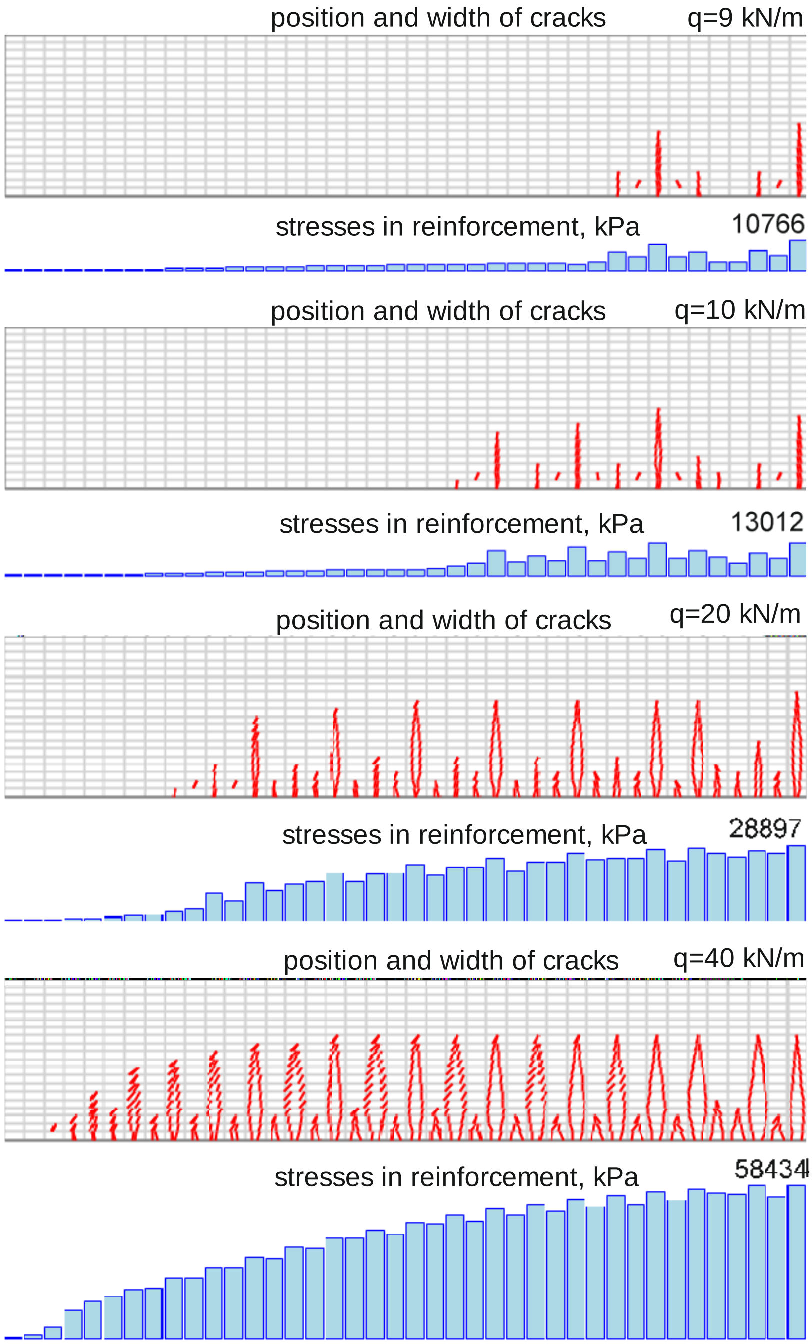

Figure 8. Position and width of cracks, and stresses in reinforcement with increasing load from q = 9 kN/m to q = 40 kN/m. The width of cracks is shown 500 times greater than the actual one.

To compare the results, beam calculations were performed using standard flat rectangular finite elements (Fig. 9). The beam was calculated for the load q = 20 kN/m after all cracks had formed. All beam parameters, including reinforcement, were taken to be the same. Along the lines, where cracks had formed, the nodes of adjacent finite elements were separated. In Fig. 9, such lines are marked in red. To simplify the calculation scheme, the slope of all cracks is taken to be 90 degrees. The reinforcement was divided by length into 40 rod finite elements (Fig. 7).

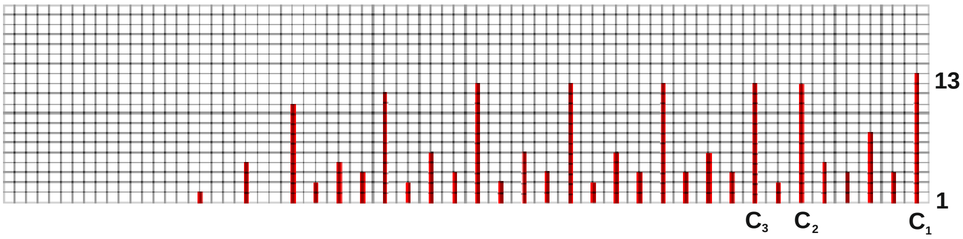

Figure 9. Standard finite element mesh. The beam is divided into 20 elements along the height and into 80 elements along the length. The red lines show the nodes separation of adjacent elements by cracks. The load is *q* = 20 kN/m.

Tables 2–4 provide the values of the opening width for cracks C_1, C_2, C_3 (Fig. 9). For standard finite elements, the data are given in the rows designated FE, and for the proposed finite elements in the rows designated Cr-FE. For standard finite elements [38], the crack width was defined as the difference in the node's displacements along the X axis of two finite elements, separated by a crack. Comparison of the results given in Tables 2–4 for the two solutions shows that they agree with high accuracy. Note that for other cracks, the same good agreement of crack opening values is observed. This indicates that the proposed finite element allows to get enough accurate determination of the crack width in the calculated structure.

Table 2. Width of crack C_1 opening from bottom to top, mm. The load value is q = 20 kN/m.

Type of FE		1	2	3	4	5	6	7	8	9	10	11	12	13
Cr-FE	down	0.016	0.022	0.027	0.032	0.034	0.033	0.031	0.029	0.026	0.022	0.018	0.013	0.007
	up	0.023	0.027	0.032	0.034	0.033	0.031	0.029	0.026	0.022	0.018	0.013	0.007	0
FE [36]	down	0.018	0.022	0.027	0.030	0.032	0.032	0.030	0.028	0.025	0.021	0.0165	0.012	0.007
	up	0.022	0.027	0.030	0.032	0.032	0.030	0.028	0.025	0.021	0.0165	0.012	0.007	0

Table 3. Width of crack C_2 opening from bottom to top, mm. The load value is q = 20 kN/m.

Type of FE		1	2	3	4	5	6	7	8	9	10	11	12
Cr-FE	down	0.012	0.022	0.030	0.037	0.041	0.040	0.036	0.032	0.027	0.022	0.016	0.010
	up	0.022	0.033	0.038	0.041	0.040	0.036	0.032	0.027	0.022	0.016	0.009	0
FE [35]	down	0.014	0.022	0.030	0.036	0.039	0.038	0.035	0.031	0.026	0.021	0.016	0.010
	up	0.022	0.030	0.036	0.039	0.038	0.035	0.031	0.026	0.021	0.016	0.010	0

Table 4. Width of crack C_3 opening from bottom to top, mm. The load value is q = 20 kN/m.

Type of FE		1	2	3	4	5	6	7	8	9	10	11	12
Cr-FE	down	0.012	0.022	0.030	0.037	0.039	0.037	0.034	0.029	0.025	0.020	0.014	0.008
	up	0.022	0.030	0.037	0.039	0.037	0.034	0.029	0.025	0.020	0.014	0.008	0
FE [36]	down	0.014	0.022	0.030	0.035	0.037	0.035	0.032	0.028	0.024	0.019	0.013	0.008
	up	0.022	0.030	0.035	0.037	0.035	0.032	0.028	0.024	0.019	0.013	0.008	0

Table 5. The comparison of calculations results.

Type of element	Vertical displacement Zmax, mm	Compressive stress $\sigma_{x,max}$, kPa	Stress in reinforcement S_{max}, kPa
Cr-FE	2.77	4538	28936
FE [36]	2.73	4575	28857

Table 5 presents the main calculation results for comparison. The comparison of the results demonstrates good agreement between the values of the maximum vertical displacement, maximum stresses in the beam compressed zone, and maximum tensile stresses in the reinforcement. The maximum displacements differ by 1.5 %, the maximum stresses in compressed concrete and reinforcement differ by less than 1 %. The crack width for the two solutions differs by no more than 5–7 %.

In this paper, the case of active loading is considered, when the cracks do not close. For the proposed finite element, taking into account the possible closing of cracks and friction forces between the crack's sides is not difficult and easily implemented. To calculate taking into account physical nonlinearity, it is necessary to change the iteration algorithm. When using the elastic solution method, we should simply use the secant modulus instead of the initial modulus of elasticity. All formulas remain the same.

4. Conclusions

1. A rectangular flat finite element is proposed that allows modeling the process of crack formation without changing the initial elements' grid. The finite element is based on the stress fields approximations and the principle of possible displacements, with the help of which the equilibrium equations of nodes are obtained. The simple linear functions are used for possible displacements. To approximate stresses, linear functions were used, ensuring the fulfillment of the equilibrium equations in the finite element region in the absence of a distributed load. To calculate the stiffness matrix of a finite element, the principle of minimum additional energy was used, to which algebraic equilibrium equations were added using the Lagrange multiplier method. After a crack formation in the center of finite element, additional degrees of freedom were introduced into its nodes, determining the possible mutual displacement of the element's parts.
2. The calculations were performed for a rectangular bending beam with a low tensile strength. The reinforcement was located in the tensile zone of the beam. The beam was divided by height into 20, and by length into 40 proposed finite elements. For comparison, the beam was also calculated using standard finite elements. In this case, the beam was divided into 80 finite elements along its length, and the nodes along the crack lines of adjacent finite elements were different. The comparison of the results, including the crack width, for the two solutions showed that they coincided with high accuracy. The test beam was calculated in an elastic setting. To calculate taking into account physical nonlinearity, it is necessary to change only the iteration algorithm. When using the elastic solution method, we should simply use the secant modulus instead of the initial modulus of elasticity. All formulas remain the same.
3. The proposed finite element can be used to calculate structures made of reinforced concrete, masonry, fiber concrete, and other materials with low tensile strength. To calculate structures with existing cracks, their position can be specified as initial data. The proposed flat finite element allows modeling the process of crack formation under load without changing the finite element mesh.

References

1. Bai, X., Wang, X. Simulation of cracking processes of the rectangular cavern surrounding rock based on a continuum–discontinuum method. Engineering Fracture Mechanics. 2024. 307. Article no. 110304. DOI: 10.1016/j.engfracmech.2024.110304
2. Ghadimi, S., Zamani-Ahari, G., Kourehli, S.S. A novel approach to crack modeling using extended finite element and substructures methods. Structures. 2024. 68. Article no. 107219. DOI: 10.1016/j.istruc.2024.107219
3. Koutromanos, I. A C^0 scalar field approach for describing sprain variables in finite element analysis of fracture. Computers & Structures. 2024. 294. Article no. 107259. DOI: 10.1016/j.compstruc.2023.107259
4. Zhou, X.-P., Chen, J.-W., Berto, F. XFEM based node scheme for the frictional contact crack problem. Computers & Structures. 2020. 231. Article no. 106221. DOI: 10.1016/j.compstruc.2020.106221
5. Deng, H., Yan, B., Koyanagi, J. Improved XFEM for 3D interfacial crack modeling. Mechanics of Materials. 2023. 186. Article no. 104811. DOI: 10.1016/j.mechmat.2023.104811
6. Scamardo, M., Franchi, A., Crespi, P. A non-standard numerical method for finite element modelling of tensile cracks in quasi-brittle material. Computers & Structures. 2022. 258. Article no. 106664. DOI: 10.1016/j.compstruc.2021.106664
7. Wang, K., Tang, C., Li, G., Zhang, H., Lu, Z. Modeling fracture problems by the local mesh refinement NMM with variable-midside-node elements. Computers & Structures. 2023. 279. Article no. 106984. DOI: 10.1016/j.compstruc.2023.106984
8. Yu, C. A coupled smeared crack-plasticity model in incremental sequentially linear analysis for mixed failure modes. Computers & Structures. 2022. 269. Article no. 106824. DOI: 10.1016/j.compstruc.2022.106824
9. Kim, U.-J., Kim, I.-G., Yun, K., Jon, M.-G., Kim, U.-B. A novel sequentially linear approach based on exponential saw-tooth softening in fracture analysis of quasi-brittle material. Computers & Structures. 2024. 297. Article no. 107317. DOI: 10.1016/j.compstruc.2024.107317
10. Češarek Kolšek, J., Planinc, I., Bratina, S. A novel family of strain-based finite elements for the analysis of the material softening of planar frames. Computers & Structures. 2024. 301. Article no. 107442. DOI: 10.1016/j.compstruc.2024.107442
11. Do, T.M.D., Lam, T.Q.K. Design parameters of steel fiber concrete beams. Magazine of Civil Engineering. 2021. 102(2). Article no. 10207. DOI: 10.34910/MCE.102.7

12. Li, Z., Zhu, H., Du, C., Gao, D., Yuan, J., Wen, C. Experimental study on cracking behavior of steel fiber-reinforced concrete beams with BFRP bars under repeated loading. Composite Structures. 2021. 267. Article no. 113878. DOI: 10.1016/j.compstruct.2021.113878
13. Nuguzhinov, Zh., Vatin, N., Bakirov, Zh., Khabidolda, O., Zholmagambetov, S., Kurokhtina, I. Stress-strain state of bending reinforced beams with cracks. Magazine of Civil Engineering. 2020. 97(5). Article no. 9701. DOI: 10.18720/MCE.97.1
14. Klochkov, Yu.V., Pshenichkina, V.A., Nikolaev, A.P., Vakhnina, O.V., Klochkov, M.Yu. Stress-strain state of elastic shell based on mixed finite element. Magazine of Civil Engineering. 2023. 120(4). Article no. 12003. DOI: 10.34910/MCE.120.3
15. Liu, H., Zhong, H. Transverse free vibration analysis of thin sectorial plates by the weak form quadrature element method. Journal of Vibration and Control. 2024. 289. Pp. 5560–5577. DOI: 10.1177/10775463231225276
16. Lukashevich, A.A. Finite element models based on the approximation of discontinuous stress fields. Magazine of Civil Engineering. 2022. 110(2). Article no. 11004. DOI: 10.34910/MCE.110.4
17. Xiao, J.-L., Nie, X., Liu, Y.-F., Fan, J.-S. Structural performance assessment of RC flexural members through crack-based fibre beam-column model updating. Computers & Structures. 2023. 281. Article no. 107029. DOI: 10.1016/j.compstruc.2023.107029
18. Dang-Trung, H., Keilegavlen, E., Berre, I. Numerical modeling of wing crack propagation accounting for fracture contact mechanics. International Journal of Solids and Structures. 2020. 204–205. Pp. 233–247. DOI: 10.1016/j.ijsolstr.2020.08.017
19. Zhao, J.W., Feng, S.Z., Tao, Y.R., Li, Z.X. Stable node-based smoothed extended finite element method for fracture analysis of structures. Computers & Structures. 2020. 240. Article no. 106357. DOI: 10.1016/j.compstruc.2020.106357
20. Khoei, A.R., Nikbakht, M. An enriched finite element algorithm for numerical computation of contact friction problems. International Journal of Mechanical Sciences. 2007. 49(2). Pp. 183–199. DOI: 10.1016/j.ijmecsci.2006.08.014
21. Peng, X., Kulasegaram, S., Bordas, S.P.A., Wu, S.C. An extended finite element method with smooth nodal stress. arXiv:1306.0536. 2013. DOI: 10.48550/arXiv.1306.0536
22. Tyukalov, Yu.Ya. Calculation of bending plates by finite element method in stresses. IOP Conference Series: Materials Science and Engineering. 2018. 451(1). Article no. 012046. DOI: 10.1088/1757-899X/451/1/012046
23. Tyukalov, Yu.Ya. Calculation of circular plates with assuming shear deformations. IOP Conference Series: Materials Science and Engineering. 2019. 687(3). Article no. 033004. DOI: 10.1088/1757-899X/687/3/033004
24. Tyukalov, Yu.Ya. Triangular prism finite element based on piecewise constant stress approximations. Magazine of Civil Engineering. 2023. 121(5). Article no. 12105. DOI: 10.34910/MCE.121.5
25. Tyukalov, Yu.Ya. Arbitrary quadrangular finite element for plates with shear deformations. Magazine of Civil Engineering. 2021. 107(7). Article no. 10707. DOI: 10.34910/MCE.107.7
26. Cunha, R.N., Amorim, D.L.N.F., Proença, S.P.B., Flórez-López, J. Modeling the initiation and propagation of complex networks of cracks in reinforced concrete plates. Engineering Structures. 2024. 308. Article no. 117993. DOI: 10.1016/j.engstruct.2024.117993
27. Luo, Y., Featherston, C.A., Kennedy, D. A hybrid model for modelling arbitrary cracks in isotropic plate structures. Thin-Walled Structures. 2023. 183. Article no. 110345. DOI: 10.1016/j.tws.2022.110345
28. Liu, J., Zhao, X.-L., Xin, H., Zhang, Y. Prediction of fatigue crack propagation in center cracked steel plate strengthened with partially covered CFRP strip. Thin-Walled Structures. 2023. 189. Article no. 110917. DOI: 10.1016/j.tws.2023.110917
29. Song, Z., Lai, S.-K., Dai, J.-G. Refined models for free vibration analysis of elastic plates with part-through surface cracks. Thin-Walled Structures. 2023. 182(B). Article no. 110312. DOI: 10.1016/j.tws.2022.110312
30. Min, Q., Li, M., Zhang, M., Lian, H., Jacquemin, T., Bordas, S.P.A. Node projection strategy for FEM simulating cross-scale crack propagation in massive concrete structures. Engineering Structures. 2023. 293. Article no. 116665. DOI: 10.1016/j.engstruct.2023.116665
31. Wang, C., Ping, X., Wang, X. An adaptive finite element method for crack propagation based on a multifunctional super singular element. International Journal of Mechanical Sciences. 2023. 247. Article no. 108191. DOI: 10.1016/j.ijmecsci.2023.108191
32. Zhou, L., Wang, J., Wang, Y., Li, X., Chai, Y. The enriched finite element method-virtual crack closure technique for cracked structures. Thin-Walled Structures. 2023. 187. Article no. 110756. DOI: 10.1016/j.tws.2023.110756
33. Tao, M.-X., Wang, Y.-L., Zhao, J.-Z. Internal force redistribution caused by cracking of concrete in composite frame structures under lateral load. Engineering Structures. 2023. 283. Article no. 115876. DOI: 10.1016/j.engstruct.2023.115876
34. Kaklauskas, G., Sokolov, A., Sakalauskas, K. Strain compliance crack model for RC beams: primary versus secondary cracks. Engineering Structures. 2023. 281. Article no. 115770. DOI: 10.1016/j.engstruct.2023.115770
35. Tyukalov, Yu.Ya. Equilibrium finite elements for plane problems of the elasticity theory. Magazine of Civil Engineering. 2019. 91(7). Pp. 80–97. DOI: 10.18720/MCE.91.8
36. Lalin, V.V., Rybakov, V.A., Diakov, S.F., Kudinov, V.V., Orlova, E.S. The semi-shear theory of V.I. Slivker for the stability problems of thin-walled bars. Magazine of Civil Engineering. 2019. 87(3). Pp. 66–79. DOI: 10.18720/MCE.87.6
37. Lalin, V.V., Rybakov, V.A., Ivanov, S.S., Azarov, A.A. Mixed finite-element method in V.I. Slivker's semi-shear thin-walled bar theory. Magazine of Civil Engineering. 2019. 89(5). Pp. 79–93. DOI: 10.18720/MCE.89.7
38. Karpilovskiy, V.S., Kriksunov, E.Z., Malyarenko, A.A., Mikitarenko, M.A., Perelmuter, A.V., Perelmuter, M.A. Vychislitelnyy kompleks SCAD [Computer complex SCAD]. Moscow: SKAD SOFT, 2009. 647 p.

Information about the author:

***Yury Tykalov**, Doctor of Technical Sciences*
ORCID: https://orcid.org/0000-0001-6184-2365
E-mail: yutvgu@mail.ru

Received: 20.09.2024; Approved: 05.04.2025; Accepted: 15.04.2025.